Numerical Differentiation for Non-Trivial Consistent Tangent Matrices: An Application to the MRS-Lade Model

A. Pérez-Foguet
A. Rodríguez-Ferran
A. Huerta

Publication CIMNE Nº 151, January 1999

Numerical Differentiation for Non-Trivial Consistent Tangent Matrices: An Application to the MRS-Lade Model

A. Pérez-Foguet
A. Rodríguez-Ferran
A. Huerta

Publication CIMNE Nº 151, January 1999

International Center for Numerical Methods in Engineering
Gran Capitán s/n, 08034 Barcelona, Spain

Numerical differentiation for non-trivial consistent tangent matrices: an application to the MRS-Lade model ⋆

Agustí PÉREZ-FOGUET, Antonio RODRÍGUEZ-FERRAN and Antonio HUERTA [1]

Departament de Matemàtica Aplicada III, E.T.S. de Ingenieros de Caminos Edifici C2, Campus Nord, Universitat Politècnica de Catalunya E-08034 Barcelona, Spain. web: `www.upc.es\ma3\lacan.html`

Abstract

In Reference [1] the authors have shown that numerical differentiation is a competitive alternative to analytical derivatives for the computation of consistent tangent matrices. Relatively simple models were treated in that reference. The approach is extended here to a complex model: the MRS-Lade model [2,3]. This plastic model has a cone-cap yield surface and exhibits strong coupling between the flow vector and the hardening moduli. Because of this, derivating these quantities with respect to stresses and internal variables —the crucial step in obtaining consistent tangent matrices— is rather involved. Numerical differentiation is used here to approximate these derivatives. The approximated derivatives are then used *1)* to compute consistent tangent matrices (global problem) and *2)* to integrate the constitutive equation at each Gauss point (local problem) with the Newton-Raphson method. The choice of the stepsize (i.e. the perturbation in the approximation schemes), based on the concept of relative stepsize, poses no difficulties. In contrast to previous approaches for the MRS-Lade model, quadratic convergence is achieved, for both the local and the global problems. The computational efficiency (CPU time) and robustness of the proposed approach is illustrated by means of several numerical examples, where the major relevant topics are discussed in detail.

Key words: consistent tangent matrices; numerical differentiation; MRS-Lade model; quadratic convergence; computational plasticity; full Newton-Raphson method

⋆ Partially supported by CICYT, Spain. Grant contract: TAP98-0421

[1] Corresponding author. e-mail: `huerta@lacan.upc.es`

7th January 1999

The main conclusion in [1] is that numerical differentiation is an efficient and robust strategy, which maintains quadratic convergence and has a very marginal CPU time overhead (with respect to analytical derivatives).

In this paper numerical differentiation is applied to compute the derivatives of a quite more complex model: MRS-Lade. In contrast to Reference [1], this model does not have all the analytical derivatives of the flow vector and the hardening moduli available. However, the same conclusions of Reference [1] are reached: robustness and efficiency.

Thus, the improvement of numerical differentiation over other techniques for the MRS-Lade model [6,7] is more clear than for simpler material models: it is the first time that quadratic convergence results are presented for the global and the local problems for this model. As a final introductory remark, it is worth noting that the MRS-Lade model is used here for illustrative purposes. The same approach can be used to compute consistent tangent matrices for other complex material models.

An outline of this paper follows. The problem is stated in Section 2. After some preliminaries on small-strain elastoplasticity, the MRS-Lade model is briefly reviewed. The proposed approach, based on numerical differentiation, is presented in Section 3. In section 4, several examples of local and global problems are discussed in detail, and the convergence results are highlighted. Finally, the main conclusions are summarized in section 5.

2 Problem statement

2.1 Preliminaries

Many elastoplastic models for small strains can be put in the general form [8]

$$\begin{aligned} \boldsymbol{\varepsilon} &= \boldsymbol{\varepsilon}^e + \boldsymbol{\varepsilon}^p \\ \boldsymbol{\sigma} &= \mathbf{E}\boldsymbol{\varepsilon}^e \\ \dot{\boldsymbol{\varepsilon}}^p &= \dot{\lambda}\mathbf{m}(\boldsymbol{\sigma}, \boldsymbol{\kappa}) \\ \dot{\boldsymbol{\kappa}} &= \dot{\lambda}\mathbf{h}(\boldsymbol{\sigma}, \boldsymbol{\kappa}) \ , \end{aligned} \tag{1}$$

where $\boldsymbol{\varepsilon}$, $\boldsymbol{\varepsilon}^e$ and $\boldsymbol{\varepsilon}^p$ are the total, elastic and plastic strain tensors respectively, $\boldsymbol{\sigma}$ is the Cauchy stress tensor, $\mathbf{E}$ is the elastic stiffness tensor, $\mathbf{m}$ is the flow vector, $\boldsymbol{\kappa}$ is the set of internal variables and $\mathbf{h}$ are the plastic moduli. The plastic multiplier $\dot{\lambda}$ is determined with the aid of the loading-unloading criterion,

where q_a, m and α are parameters of the model, $g(\theta)$ is the Willam-Warnke function, $\eta_{con}(\kappa_{con})$ is a hardening/softening function related with the friction angle, and $p_{cap}(\kappa_{cap})$ is a hardening function related with the triaxial compression strength. The definitions of $g(\theta)$, $\eta_{con}(\kappa_{con})$ and $p_{cap}(\kappa_{cap})$ are in Appendix A. The trace of F_{con} and F_{cap} in the meridian plane and in the deviatoric plane are depicted in Figure 1. The nonlinear shape of the hardening/softening function $\eta_{con}(\kappa_{con})$ is shown in Figure 2.

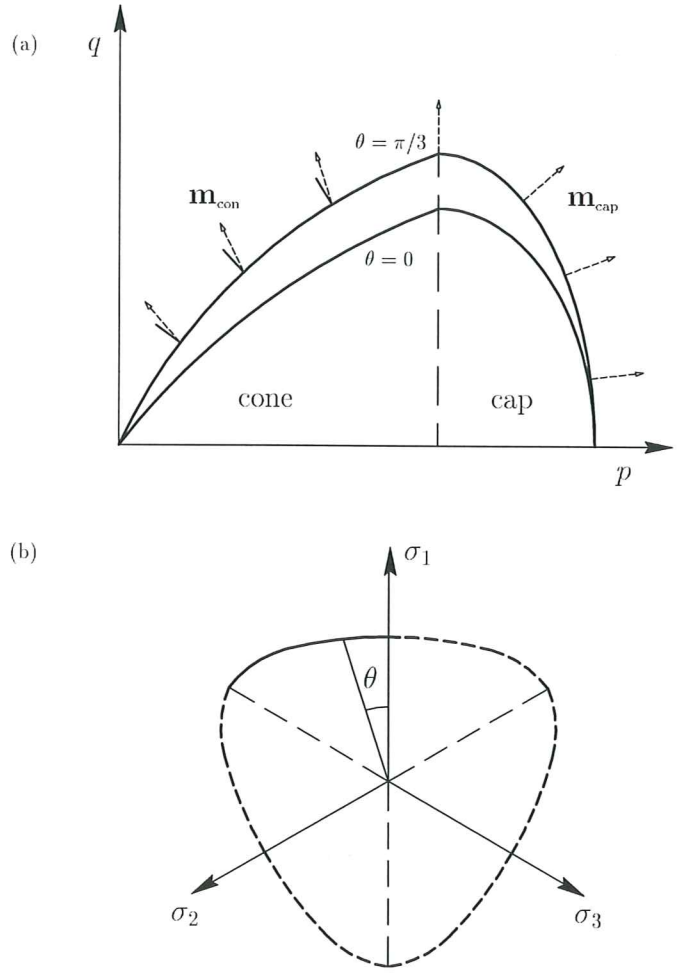

Figure 1. MRS-Lade model. Trace of the yield criterion: (a) on the meridian plane; (b) on the deviatoric plane

The plastic flow vector $\mathbf{m}$ is also defined in two parts, cone and cap:

$$\mathbf{m}(\boldsymbol{\sigma}, \kappa_{con}, \kappa_{cap}) = \begin{cases} \mathbf{m}_{con} = \mathbf{A}\mathbf{n}_{con} & \text{if} \quad p \leq \alpha p_{cap}(\kappa_{cap}) \\ \mathbf{m}_{cap} = \mathbf{n}_{cap} & \text{if} \quad p > \alpha p_{cap}(\kappa_{cap}) \end{cases} \tag{5}$$

Combining equations (7), (8) and the last equation in (1) shows that the hardening moduli $\mathbf{h} = (h_{\text{con}}, h_{\text{cap}})$ are

$$\begin{aligned} h_{\text{con}}(\boldsymbol{\sigma}, \kappa_{\text{con}}, \kappa_{\text{cap}}) &= \frac{1}{c_{\text{con}} p_{\text{a}}} \left(\frac{p}{p_{\text{a}}} \right)^{-l} \boldsymbol{\sigma}^t \mathbf{m} \\ h_{\text{cap}}(\boldsymbol{\sigma}, \kappa_{\text{con}}, \kappa_{\text{cap}}) &= \frac{1}{c_{\text{cap}} p_{\text{a}}} \left(\frac{p_{\text{cap},0}}{p_{\text{a}}} \right)^{-r} \boldsymbol{\sigma}^t \mathbf{m} \,. \end{aligned} \tag{9}$$

Equations (5), (6) and (9) clearly exhibit a complex dependence of the flow vector $\mathbf{m}$ and the hardening moduli $\mathbf{h}$ with respect to the stresses $\boldsymbol{\sigma}$ and the internal variables $\boldsymbol{\kappa}$. This makes the efficient time-integration of the MRS-Lade model a challenging issue, as discussed in the following.

3 Proposed approach

3.1 Numerical time-integration: the local and global problems

Time-integration of equation (1) with the backward Euler scheme yields the following nonlinear local problem [8,9]:

$$\begin{aligned} {}^{n+1}\boldsymbol{\sigma} + \lambda \mathbf{E} \mathbf{m}({}^{n+1}\boldsymbol{\sigma}, {}^{n+1}\boldsymbol{\kappa}) &= \mathbf{E}({}^{n+1}\boldsymbol{\varepsilon} - {}^{n}\boldsymbol{\varepsilon}^p) \\ {}^{n+1}\boldsymbol{\kappa} - \lambda \mathbf{h}({}^{n+1}\boldsymbol{\sigma}, {}^{n+1}\boldsymbol{\kappa}) &= {}^{n}\boldsymbol{\kappa} \\ F({}^{n+1}\boldsymbol{\sigma}, {}^{n+1}\boldsymbol{\kappa}) &= 0 \,. \end{aligned} \tag{10}$$

In equation (10), the state at time t_n (i.e., quantities ${}^{n}\boldsymbol{\varepsilon}^p$ and ${}^{n}\boldsymbol{\kappa}$) and the *total* strains ${}^{n+1}\boldsymbol{\varepsilon}$ at time t_{n+1} are known. The unknowns of this local problem are the stresses ${}^{n+1}\boldsymbol{\sigma}$ and the internal variables ${}^{n+1}\boldsymbol{\kappa}$ at time t_{n+1}, and the incremental plastic multiplier λ.

To solve this nonlinear local problem with the Newton-Raphson method the Jacobian of the residual is needed. Using standard vector notation of computational mechanics [11] and dropping the superscript $n+1$ the Jacobian can be written as

$$\mathbf{J} = \begin{pmatrix} \left(\mathbf{I}_{\dim(\sigma)} + \lambda \mathbf{E} \frac{\partial \mathbf{m}}{\partial \boldsymbol{\sigma}} \right) & \lambda \mathbf{E} \frac{\partial \mathbf{m}}{\partial \boldsymbol{\kappa}} & \mathbf{m} \\ -\lambda \frac{\partial \mathbf{h}}{\partial \boldsymbol{\sigma}} & \left(\mathbf{I}_{\dim(\kappa)} - \lambda \frac{\partial \mathbf{h}}{\partial \boldsymbol{\kappa}} \right) & -\boldsymbol{\kappa} \\ \mathbf{n}^t & \boldsymbol{\xi}^t & 0 \end{pmatrix} \tag{11}$$

where $\mathbf{n}$ and $\boldsymbol{\xi}$ are the derivatives of $F(\boldsymbol{\sigma}, \boldsymbol{\kappa})$ with respect to $\boldsymbol{\sigma}$ and $\boldsymbol{\kappa}$ respectively, and $\dim(\kappa)$ is the number internal variables (i.e. $\dim(\kappa) = 2$ for the MRS-Lade model).

notation is used), for instance, is approximated either by

$$\begin{aligned}
\text{1ND-O}(h) \qquad & \frac{\partial m_i}{\partial \kappa_j}(\boldsymbol{\sigma}, \boldsymbol{\kappa}) = \frac{m_i(\boldsymbol{\sigma}, \boldsymbol{\kappa} + h\mathbf{e}_j) - m_i(\boldsymbol{\sigma}, \boldsymbol{\kappa})}{h}, \\
\text{1ND-O}(h^2) \qquad & \frac{\partial m_i}{\partial \kappa_j}(\boldsymbol{\sigma}, \boldsymbol{\kappa}) = \frac{m_i(\boldsymbol{\sigma}, \boldsymbol{\kappa} + h\mathbf{e}_j) - m_i(\boldsymbol{\sigma}, \boldsymbol{\kappa} - h\mathbf{e}_j)}{2h}, \\
\text{1CND-O}(h^2) \qquad & \frac{\partial m_i}{\partial \kappa_j}(\boldsymbol{\sigma}, \boldsymbol{\kappa}) = \frac{\mathrm{Im}(m_i(\boldsymbol{\sigma}, \boldsymbol{\kappa} + \sqrt{-1}h\mathbf{e}_j))}{h},
\end{aligned} \tag{13}$$

where h is the stepsize and $\mathbf{e}_j$ is the jth unit vector. Similar expressions are used for $\partial\mathbf{m}/\partial\boldsymbol{\sigma}$, $\partial\mathbf{h}/\partial\boldsymbol{\sigma}$ and $\partial\mathbf{h}/\partial\boldsymbol{\kappa}$. The approximated derivatives are then used to solve the local and the global problems.

Notation	Description
1ND-O(h)	Forward difference scheme (1^{st} order accurate)
1ND-O(h^2)	Centered difference scheme (1^{st} order accurate)
1CND-O(h^2)	Approximation based on complex variables (2^{nd} order accurate)

Table 1
Numerical approximations to first derivatives

A crucial issue in numerical differentiation is the choice of the stepsize h. In this work it is selected as shown in Reference [1], by using the concept of *relative* stepsize, h_r. The optimal value of the relative stepsize can be approximated by $\sqrt{\texttt{macheps}}$ for the first-order scheme, 1ND-O(h), and by $\sqrt[3]{\texttt{macheps}}$ for the second-order accurate schemes, 1ND-O(h^2) and 1CND-O(h^2), with `macheps` the machine precision.

Numerical experiments reveal a good behaviour of numerical differentiation (that is, quadratic convergence for both the local and the global problems) for a wide range of relative stepsizes, h_r. In order to reduce the effect of rounding errors, h_r is taken as a negative power of 2 ($h_r = 2^{-k}$), not of 10 ($h_r = 10^{-k}$). This choice is relevant in some critical zones, as illustrated in next section.

5 Examples

In this section, several local and global problems are solved quadratically with numerical differentiation. The three techniques of Table 1 are compared and the main features of each one are remarked.

Two sets of parameters have been used, see Table 2. Soil S1 is a dense Sacramento River sand [7]. Soil S2 is a small modification of soil S1. The modifications are *1)* a smaller value of $\bar{\eta}_{\text{con}}$, which reduces the size of the elastic

In order to show that quadratic convergence is obtained in all stress–internal variable space, three different deformation paths are considered. The paths are characterized by an initial stress–internal variable state, $\boldsymbol{\sigma}_{\text{ini}}$ and $\boldsymbol{\kappa}_{\text{ini}}$, and a total strain increment, $\Delta\boldsymbol{\varepsilon}$ (applied in 50 steps) see Table 3. The material parameters of soil S2 have been used.

	Path A	Path B	Path C
$\boldsymbol{\sigma}_{\text{ini}}$	$(1000, 1000, 1000, 0)$	$(4800, 4800, 4800, 0)$	$(4800, 4800, 4800, 0)$
$\boldsymbol{\kappa}_{\text{ini}}$	$(0, 0)$	$(0, 0)$	$(0, 0)$
$\Delta\boldsymbol{\varepsilon}$	$(0, 0, 0, 0.2)$	$(0, 0, 0, 0.2)$	$(-0.1, 0, 0, 0)$
n	50	50	50

Table 3
Definition of the three stress paths for the local problems

In Figure 3 the trace on the meridian plane of the three stress paths and the trace of the initial and final yield criteria are depicted. Paths A and B correspond to pure shear deformation, see $\Delta\boldsymbol{\varepsilon}$ in Table 3. Path A develops in the cone region, and path B starts in the cap region and then changes to the cone region. Path C corresponds to uniaxial compression, see Table 3, and it develops in the cap region. In Table 4 the evolution of the Lode angle, θ, is shown. Note that, in general, the paths are three–dimensional curves in the three–invariant space (p, q, θ). Indeed, θ changes during loading in paths A and B. For path C, on the other hand, θ remains constant and equal to $\pi/3$. Finally, note that the three paths start in hardening regime and finish during softening. Therefore, a wide range of different local problems is covered.

Step	1	5	10	25	50
Path A	40.3	51.5	53.1	54.1	53.9
Path B	30.0	35.8	42.2	54.7	54.1
Path C	60.0	60.0	60.0	60.0	60.0

Table 4
Evolution of the Lode angle θ (in degrees) during the three stress paths defined in Table 3

In the following, quadratic convergence results are presented and analyzed for moderate strain increments. After that, the behaviour of the three numerical differentiation schemes, see Table 1, is compared. Finally, quadratic convergence results for large excursions outside the elastic domain are also shown.

5.1.1 Convergence illustration

The convergence results for different steps of the three stress paths are depicted in Figure 4. These results correspond to local problems in the cone and the cap

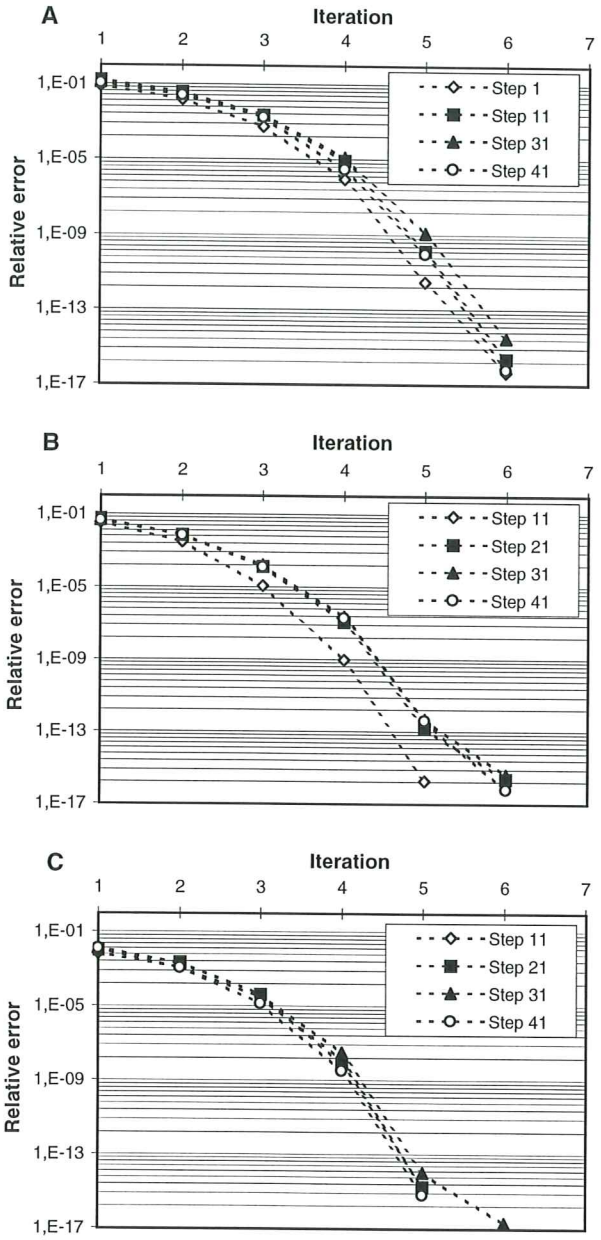

Figure 4. Convergence results for various steps of paths A, B and C

5.1.2 Comparison of numerical differentiation schemes

The three numerical differentiation schemes of Table 1 have been compared through the integration of paths A, B and C defined in Table 3.

The convergence results of step 31 of path A with different relative stepsizes h_r are depicted in Figure 7. They are quadratic up to a tolerance of 10^{-14} for a wide range of h_r with the three schemes. The same results are obtained with the other steps of paths A and B. In Table 5, the ranges of h_r that give

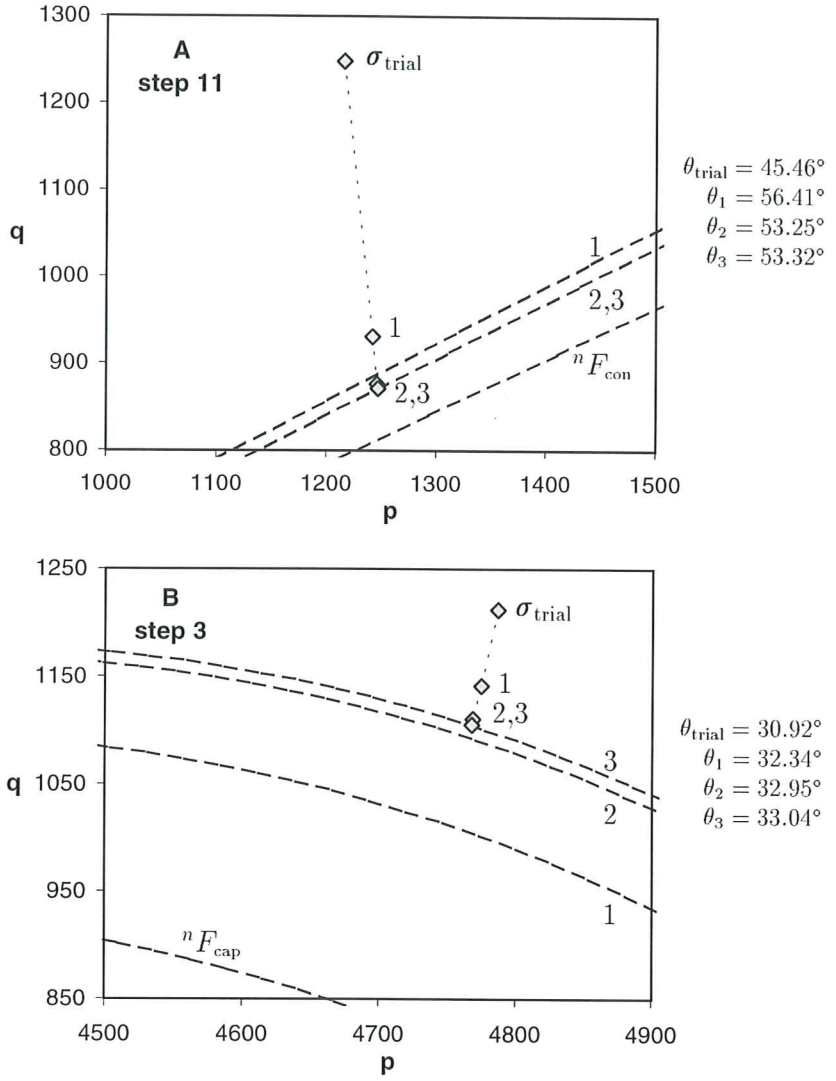

Figure 6. Evolution of the stress invariants and the yield criterion during the iterations of step 11 of path A and step 3 of path B

Num. approx.	$h_r = 10^{-k}$	$h_r = 2^{-k}$
1ND-O(h)	$10^{-5} - 10^{-6}$	$10^{-5} - 10^{-8}$
1ND-O(h^2)	$10^{-3} - 10^{-7}$	$10^{-3} - 10^{-7}$
1CND-O(h^2)	$10^{-4} - 10^{-9}$	$10^{-4} - 10^{-9}$

Table 6
Range of relative stepsizes h_r that give quadratic convergence in the local problem, stress path C

5.1.3 Large excursions outside the elastic domain

In order to show that quadratic convergence is also attained for large excursions outside the elastic domain, path A defined in Table 3 is solved with only

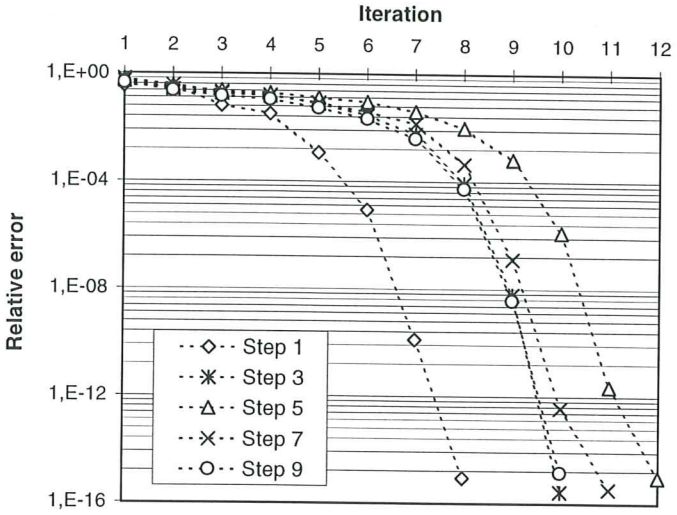

Figure 8. Convergence results for path A with only 10 steps

be attained in a simple manner with any of the three techniques of numerical differentiation. This is valid for any stress path (cone and cap regions, hardening and softening regimes), and for both moderate and large steps. The choice of the stepsize presents no difficulties, because quadratic convergence is obtained for a wide range of relative stepsizes.

5.2 Global problems

In this subsection, numerical differentiation is applied to solve several boundary value problems (i.e., global problems). That is, the numerical approximations of Table 1 are employed to compute consistent tangent matrices, see equation (12). Moreover, they are also used to solve the corresponding local problems.

Three examples are presented: the vertical displacement of a pile, a triaxial test with an homogeneous sample and a triaxial test with a non-homogeneous sample. These examples illustrate that the three numerical approximations to first derivatives of the flow vector and the hardening moduli, see Table 1, are useful to solve the global problem with quadratic convergence. Moreover, their main features (range of adequate relative stepsizes and computational cost) are compared.

5.2.1 Vertical displacement of a pile

The first example is the vertical displacement of a pile. The definition of the problem is presented by Potts and Gens [14], and it is only summarized here.

7, the ranges of h_r that give quadratic convergence during all the test are summarized.

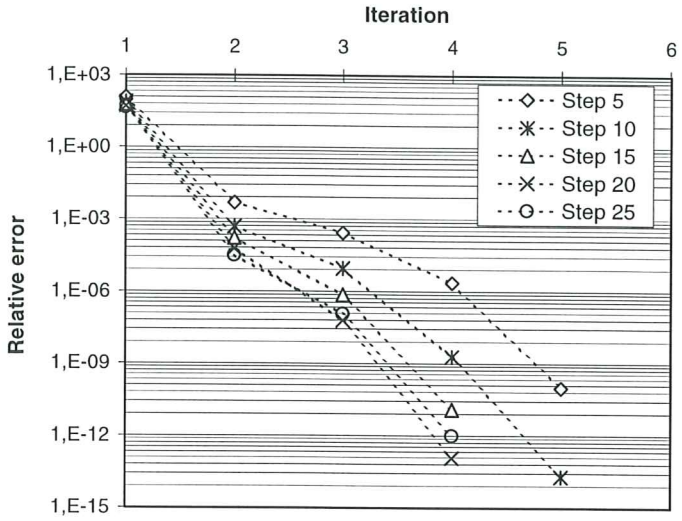

Figure 11. Convergence results for various load steps of the pile problem

Num. approx.	Range of h_r
1ND-O(h)	$10^{-5} - 10^{-9}$
1ND-O(h^2)	$10^{-3} - 10^{-9}$
1CND-O(h^2)	$10^{-3} - 10^{-9}$

Table 7
Range of relative stepsizes h_r that give quadratic convergence up to a tolerance of 10^{-10} in the pile problem

In Table 8 the computational cost (CPU time) of the three techniques with several h_r is summarized. The values are given in % with respect to 1ND-O(h) with $h_r = 10^{-8}$. The number of iterations during all the load process is equal for all the entries in Table 8, except for 1ND-O(h) with $h_r = 10^{-3}$ and 10^{-4} (which require 6 and 1 extra iterations respectively). The results are quite independent of h_r and are mainly related with the derivation technique. The 1ND-O(h^2) and 1CND-O(h^2) approximations are respectively 20% and 40% more expensive than the 1ND-O(h) approximation. These results are in agreement with the fact that the cost of a complex function evaluation can be approximated (when additions and products are balanced) by the cost of four real function evaluations. Thus, the overhead of complex approximation (one complex evaluation of the flow vector and the hardening moduli) is twice that of centered differences (that needs two real evaluations).

Quadratic convergence results have been obtained without difficulties in a simple global problem. There are not significative differences between the convergence results of the three techniques. The ranges of optimal relative stepsize

two phases: first the sample is precompressed, and second a vertical displacement is imposed at the top. A structured mesh of 150 (10×15) elements has been used. In Figure 13, the relationship between q and the axial strain for several precompressions is depicted. They coincide with those presented in [7].

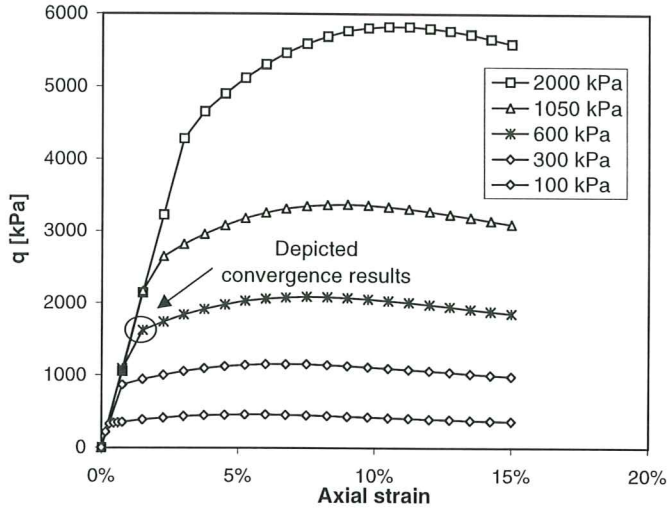

Figure 13. Invariant q versus axial strain curves for the homogeneous triaxial problem with various precompressions

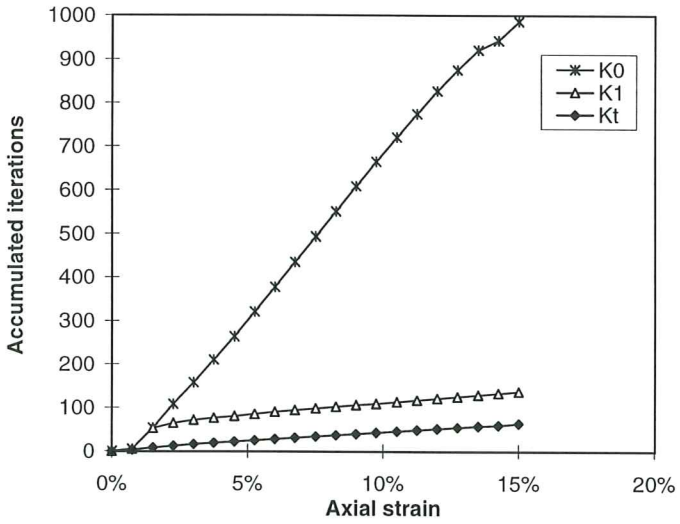

Figure 14. Accumulated iterations versus load level for the homogeneous triaxial problem with three nonlinear solvers: initial stress method (K0), modified Newton-Raphson method (K1) and full Newton-Raphson method (Kt)

In the following, attention is focused in the test with a precompression of 600 kPa. In Figure 14 three nonlinear solvers are compared, by showing the accumulated iterations versus the axial strain relationship. The advantage of using the consistent tangent matrix is clear: the number of iterations needed with the full (Kt) or modified (K1) Newton-Raphson methods is much lower

Num. approx.	Range of h_r
1ND-O(h)	$10^{-3} - 10^{-5}$
1ND-O(h^2)	$10^{-3} - 10^{-5}$
1CND-O(h^2)	$10^{-3} - 10^{-7}$

Table 9
Range of relative stepsizes h_r that give quadratic convergence in the homogeneous triaxial problem up to a tolerance of 10^{-8} (1ND-O(h) approximation) or 10^{-10} (the other two)

The convergence results of Figure 15 show that the first-order scheme, 1ND-O(h), keeps quadratic convergence up to a tolerance of 10^{-8}, and that second-order schemes reach a tolerance of 10^{-10}. This difference is due to the fact that the Lode angle θ is equal to $\pi/3$ for all the Gauss points (recall that the global problem is homogeneous). This region of stress space is the most demanding one for approximating the derivatives of the flow vector. For this reason, the differences between order 1 and order 2 in the truncation error are clear. However, it must be noted that the indicated tolerances are very strict for any practical application. Thus, even the 1ND-O(h) approximation is accurate enough if a tolerance of, say, 10^{-6} is used. With this tolerance, the three techniques provide quadratic convergence for a wide range of relative stepsizes.

5.2.3 Triaxial test: non-homogeneous sample

The third example is the triaxial test with an non-homogeneous sample. A structured mesh of 600 (20×30) elements, the material parameters of soil S2 and a precompression of 600 kPa have been used. The finite element in the the bottom left corner is weakened (the values of $\bar{\eta}_{\text{con}}$ and $p_{\text{cap},0}$ are 10% lower) to induce a non-homogeneous response.

The evolution of the second invariant of the deviatoric part of the strain tensor is depicted in Figure 16. Note that the axisymmetric nature of the test prevents localization [15].

Figure 17 shows the evolution of the load and the number of Gauss points which undergo plastic loading versus displacement. Note that after the limit load, a large reduction of number of Gauss points under plastic loading is found. Several Gauss points that were on plastic loading change to elastic unloading. Therefore, this part of the example is called *partial unloading*. During partial unloading, the mechanical behaviour of the sample becomes clearly non-homogeneous.

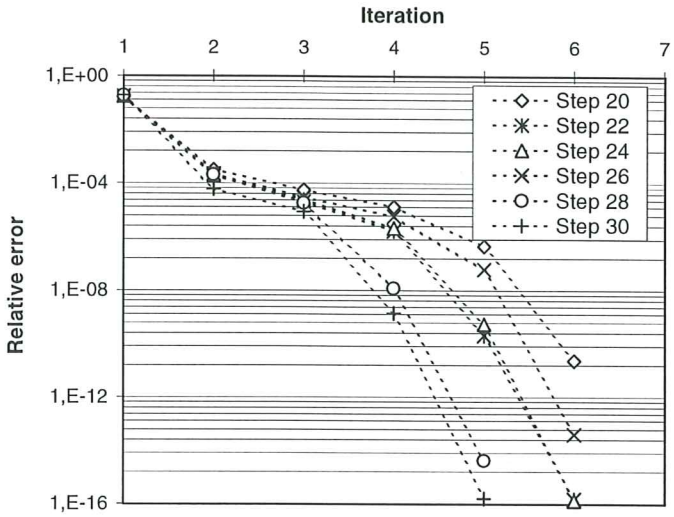

Figure 18. Convergence results for various load steps of the non-homogeneous triaxial problem

The convergence results for several load steps during partial unloading is depicted in Figure 18. Note that quadratic convergence is found. These results are obtained with the technique 1CND-O(h^2), with $h_r = 10^{-5}$ and with a tolerance of 10^{-10}. In these steps, the same results are found with the other techniques and other relative stepsizes h_r.

However, if a too strict tolerance is imposed, the convergence results obtained during the hardening regime depend on the differentiation technique and the relative stepsize. It has been already shown for the homogeneous triaxial test that the first-order technique only ensures quadratic convergence up to a tolerance of 10^{-8}. In order to check the behaviour of the three techniques with this example, the number of accumulated iterations along all the loading process with several h_r are summarized in Table 10. Two tolerances are considered: 10^{-8} and 10^{-10}.

Table 10(a) shows that, with a tolerance of 10^{-8}, the three techniques need a very similar number of iterations for a wide range of relative stepsizes. This indicates quadratic convergence in all the entries of the table. On the other hand, only the 1CND-O(h^2) approximation ensures quadratic convergence up to a tolerance of 10^{-10} during all the loading, see Table 10(b). For the other two approximations, there are variations in the number of iterations, caused by a loss of quadratic convergence.

A comparison of the computational cost (CPU time) of the three techniques with a tolerance of 10^{-10} and with several h_r is presented in Table 11. The values are given in % with respect to 1ND-O(h) with $h_r = 10^{-6}$. The forward difference scheme has a relative cost of 100 — 110%, the centered difference

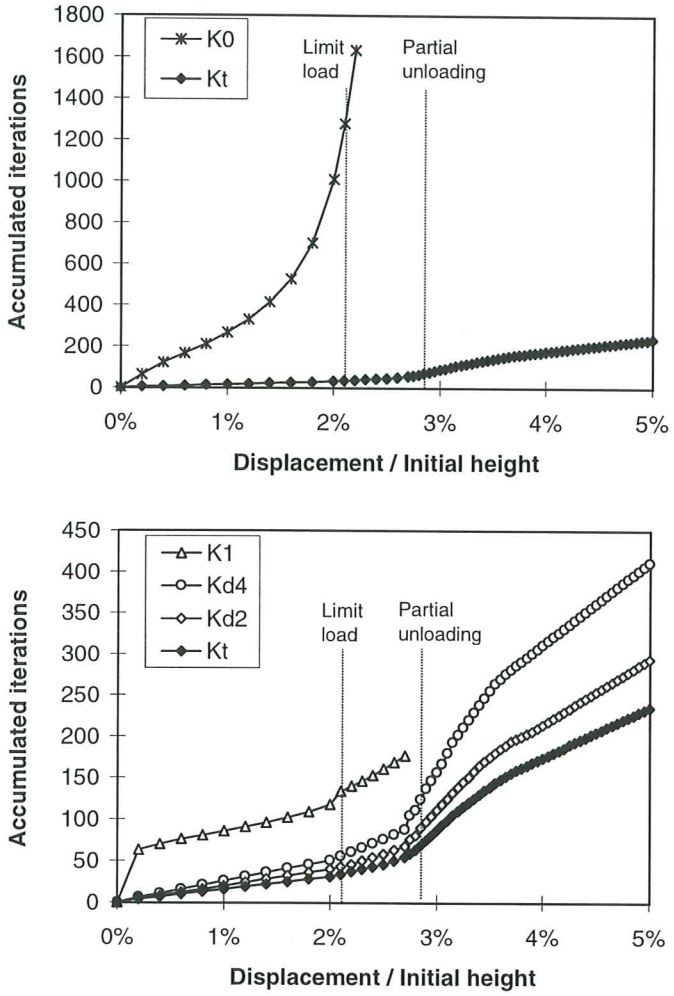

Figure 19. Accumulated iterations versus load level for the non-homogeneous triaxial problem with various nonlinear solvers

Moreover, the approximated derivatives are also used to compute the Jacobian of the residual of the local problem (time-integration of the elastoplastic constitutive equations at each Gauss point). Thus, a full Newton-Raphson method can be applied over stresses and internal variables, and quadratic convergence is also obtained.

The proposed approach has been illustrated with a complex material model: the MRS-Lade model. It is a cap-cone model with highly nonlinear hardening/softening laws. Analytical derivatives of the flow vector and the hardening moduli are not available in the literature. In fact, it is first time that quadratic convergence results are presented for this model (both for local and global problems). Extension to other complex material models is straightforward, and consists only in changing the definition of the flow vector and the hardening moduli.

[9] J. C. Simo and T. J. R. Hughes. *Computational inelasticity.* Springer-Verlag, 1998.

[10] A. Pérez-Foguet and A. Huerta. Plastic flow potential for the cone region of the MRS–Lade model. Accepted in *Journal of Engineering Mechanics*, June 1998.

[11] M. A. Crisfield. *Non-linear finite element analysis of solids and structures. 1 Essentials.* John Wiley & Sons, Chichester, 1991.

[12] K. Runesson, A. Samuelsson, and L. Bernspang. Numerical technique in plasticity including solution advancement control. *International Journal for Numerical Methods in Engineering*, 22:769–788, 1986.

[13] M. Ortiz and J. B. Martin. Symmetry-preserving return mapping algorithms and incrementally extremal paths: a unification of concepts. *International Journal for Numerical Methods in Engineering*, 28:1839–1853, 1989.

[14] D. M. Potts and A. Gens. A critical assessment of methods of correcting for drift from the yield surface in elasto-plastic finite element analysis. *International Journal for Numerical and Analytical Methods in Geomechanics*, 9:149–159, 1985.

[15] J.W. Rudnicki and J.R. Rice. Conditions for the localization of deformation in pressure-sensitive dilatant materials. *Journal of the Mechanics and Physics of Solids*, 23:371–394, 1975.

A Appendix

In the following, the formulas needed to compute the flow vector and the hardening/softening moduli that have not been presented in Subsection 2.2 are summarized.

The model is expressed through the following three invariants:

$$p = -\frac{1}{3} I_1 \quad q = \sqrt{3\, J_2} \quad \theta = \frac{1}{3} \arccos\left(\frac{3\sqrt{3} J_3}{2 J_2^{3/2}}\right) \tag{A.1}$$

with

$$I_1 = \boldsymbol{\sigma}^t \boldsymbol{\delta} \quad J_2 = \frac{1}{2} \mathbf{s}^t \mathbf{L}\, \mathbf{s} \quad J_3 = \det[\mathbf{s}] \tag{A.2}$$

where $\mathbf{s} = \boldsymbol{\sigma} + p\, \boldsymbol{\delta}$, $\mathbf{L}$ is a diagonal matrix with the diagonal terms equal to $\{1, 1, 1, 2, 2, 2\}$ (in three-dimensional problems), and $\det[*]$ is the determinant of $*$.

and the partial derivatives of F_{cap} are

$$\begin{aligned}
\frac{\partial F_{\text{cap}}}{\partial p} &= 2\,\frac{p - p_{\text{m}}}{p_{\text{r}}^2} \\
\frac{\partial F_{\text{cap}}}{\partial q} &= \frac{2\,q\,g(\theta)^2}{f_{\text{r}}^2}\left(1 + \frac{q}{q_{\text{a}}}\right)^{2m}\left(1 + \frac{m\,q}{q_{\text{a}} + q}\right) \\
\frac{\partial F_{\text{cap}}}{\partial \theta} &= \frac{2\,q^2\,g(\theta)}{f_{\text{r}}^2}\left(1 + \frac{q}{q_{\text{a}}}\right)^{2m}\frac{\partial g(\theta)}{\partial \theta}\,.
\end{aligned} \tag{A.9}$$